Taxonomy of neural oscillation events in primate auditory cortex

Samuel A Neymotin[1], Annamaria Barczak[1], Monica N. O'Connell[1], Tammy McGinnis[1], Noah Markowitz[2] , Elizabeth Espinal[2], Erica Griffith[3], Haroon Anwar[1], Salvador Dura-Bernal[1,3], William W Lytton[3,4], Stephanie R Jones[5], Stephan Bickel[1,2], Peter Lakatos[1]

[1]Center for Biomedical Imaging and Neuromodulation, Nathan Kline Institute for Psychiatric Research Orangeburg, NY
[2]Dept. Neurology and Neurosurgery, The Feinstein Institutes for Medical Research and Northwell Health Manhasset, NY
[3]Dept. Physiology and Pharmacology, SUNY Downstate Medical Center, Brooklyn, NY
[4]Dept. Neurology, Kings County Hospital Center, Brooklyn, NY
[5]Dept. Neuroscience & Carney Institute for Brain Science, Brown University, Providence, RI

Abstract

Electrophysiological oscillations in neocortex have been shown to occur as multi-cycle events, with onset and offset dependent on behavioral and cognitive state. To provide a baseline for state-related and task-related events, we quantified oscillation features in resting-state recordings. We used two invasively-recorded electrophysiology datasets: one from human, and one from non-human primate auditory system. After removing event related potentials, we used a wavelet transform based method to quantify oscillation features. We identified about 2 million oscillation events, classified within traditional frequency bands: delta, theta, alpha, beta, gamma, high gamma. Oscillation events of 1-44 cycles were present in at least one frequency band in 90% of the recordings, consistent across human and non-human primate. Individual oscillation events were characterized by non-constant frequency and amplitude. This result naturally contrasts with prior studies which assumed such constancy, but is consistent with evidence from event-associated oscillations. We measured oscillation event duration, frequency span, and waveform shape. Oscillations tended to exhibit multiple cycles per event, verifiable by comparing filtered to unfiltered waveforms. In addition to the clear *intra*-event rhythmicity, there was also evidence of *inter*-event rhythmicity within bands, demonstrated by finding that coefficient of variation of interval distributions and Fano Factor measures differed significantly from a Poisson distribution assumption. Overall, our study demonstrates that rhythmic oscillation events dominate auditory cortical dynamics.

Introduction

Intrinsic cortical oscillations consist of both rhythmic and brief pulse-like neuronal activity patterns which co-occur in electrophysiological recordings [1,2]. These patterns manifest differently across multiple frequency bands and different brain regions during various task-dependent brain states [3]. These nearly-continuous neural oscillations can be viewed as providing a background context on top of which behaviorally and cognitively relevant information (content) is transmitted [4].

Two related theories address the role of oscillations. *Entrainment theory* posits that attentional selection involves phase reset in response to relevant sensory or internal inputs; phase alignment provides optimal response to relevant time-varying signals [1,4–7]. Similarly, *communication through coherence* posits that synchronization of oscillation phase across different brain circuits optimizes the ability of the networks to transmit and receive information [8]. The presence of nearly continuous oscillations at particular frequencies (*e.g.,* gamma) is important for these mechanisms to work, since this provides the context for *sender* and *receiver* networks to periodically communicate [9–11]. Intrinsic oscillations should be distinguished from stereotypical event related potential (ERP) waveforms, which may also be prolonged enough to produce a single cycle of oscillation.

Delta (0.5-3 Hz), theta (4-8 Hz), beta (15-30 Hz), gamma (30-100 Hz), and higher frequency oscillations have been shown to occur as multi-cycle events, with onset and offset dependent on behavioral and cognitive state [4,12]. A prominent example is the primate alpha rhythm (9-14 Hz) observed in primary visual cortex [13]. This type of alpha rhythm has also been observed in primary auditory, somatosensory, and motor cortices [14–18].

The presence of high spectral power in a neural signal does not necessarily indicate an intrinsic oscillation. This is true particularly for one- or two-cycle events which could arise stochastically [2,19]. For example, a high-amplitude, single-cycle waveform with 50 ms duration could be mistaken for a 20 Hz oscillation [2,20]. If underlying neural generators are stochastic, high spectral power may simply reflect intrinsic temporal domain features from synaptic time constants or other sources [2,19]. Recent studies that support this interpretation demonstrated recurring brief events in high-frequency gamma [21,22], and in beta [20,23,24] ranges. Therefore, care must be taken to distinguish non-oscillation waveforms due to time-domain features from clear multi-cycle oscillations. The relevance of this dichotomy for particular frequency bands, particular behavioral conditions, and particular brain regions remains to be determined.

Our aim was to examine spontaneous neuronal activity, recorded over long time scales (minutes) in the awake, resting state condition in humans and non-human primates (NHPs), in order to better understand basic features and temporal properties of physiologically-relevant oscillations in auditory cortex (A1). We used two invasively-recorded electrophysiology datasets: 1) laminar local field potential (LFP) recordings from NHP A1; and 2) intracranial electroencephalogram (iEEG) recordings from human superior temporal gyrus (STG). We extracted moderate to high-power oscillation events from wavelet transform spectrograms (4× median cutoff; 7-cycle Morlet wavelets), and determined their basic properties including temporal and frequency span, peak frequency, peak power, number of cycles, number of local peaks in filtered waveforms, correlation of filtered and raw signal, and rhythmicity across individual events. To avoid contamination by evoked responses, we excluded events which matched event related potential (ERP) waveforms produced in response to auditory stimuli (normalized cross-correlation >= 0.8, and matching durations).

Our analysis revealed clear evidence of multi-cycle events in all frequency ranges (average: 3-4 cycles per event, range: 0.3-44 cycles per event), which could be seen in the unfiltered waveforms. Event occurrence in each frequency band also demonstrated rhythmicity, quantified through an analysis of interevent intervals. Overall, our data and analyses demonstrate that multi-cycle oscillation events are prominent in auditory cortex spontaneous dynamics, and that these oscillations recur quasi-rhythmically over time.

Results

Validation of *OEvent* package for oscillation event detection

We developed the *OEvent* package for the analysis of electrophysiological oscillation event features. We validated *OEvent* by measuring its accuracy in detecting the number of cycles in a simulated dataset of 10 Hz alpha sinusoidal signals. Oscillation length was varied from 1-15 cycles with a constant 3 s interval between event initiation. 39 alpha signal events were superimposed on a 117 s NHP cortex supragranular current source density (CSD) signal to provide realistic physiological background signal statistics (**Fig. 1**).

As expected, a single cycle alpha event was difficult to detect correctly (**Fig. 1A,B**). In this example, the random placement of the single cycle was such that it was immediately followed by an intrinsic cycle of comparable frequency, something that can readily occur randomly in this oscillation rich environment. Unsurprisingly, OEvent detected 2.3 cycles and over-estimated the peak frequency relative to the added cycle (12.75 Hz). An additional factor for overestimation of

both frequency and number of cycles were the sharp discontinuity transients at beginning and end associated with superimposing signal on background.

OEvent was more accurate in estimating the properties of more prolonged oscillation events: an 11-cycle alpha event was calculated as 11.7 cycles, with frequency calculated as 10.25 Hz (**Fig. 1A,C**). Accuracy was excellent across all cycle lengths with RMS error <1 (**Fig. 1D**). As in the case of **Fig 1A**, number of cycles was typically overestimated for one- and two-cycle events. Performance improved as the number of cycles in the simulated signal increased. Frequency estimation accuracy also varied with the number of cycles (**Fig. 1E**). At a low number of simulated cycles, the peak frequency was more strongly overestimated, which also contributed to overestimation of number of cycles, based on duration and frequency. Similar results for the features displayed in **Fig. 1** were obtained when embedding the alpha signal in a background of pink noise (not shown).

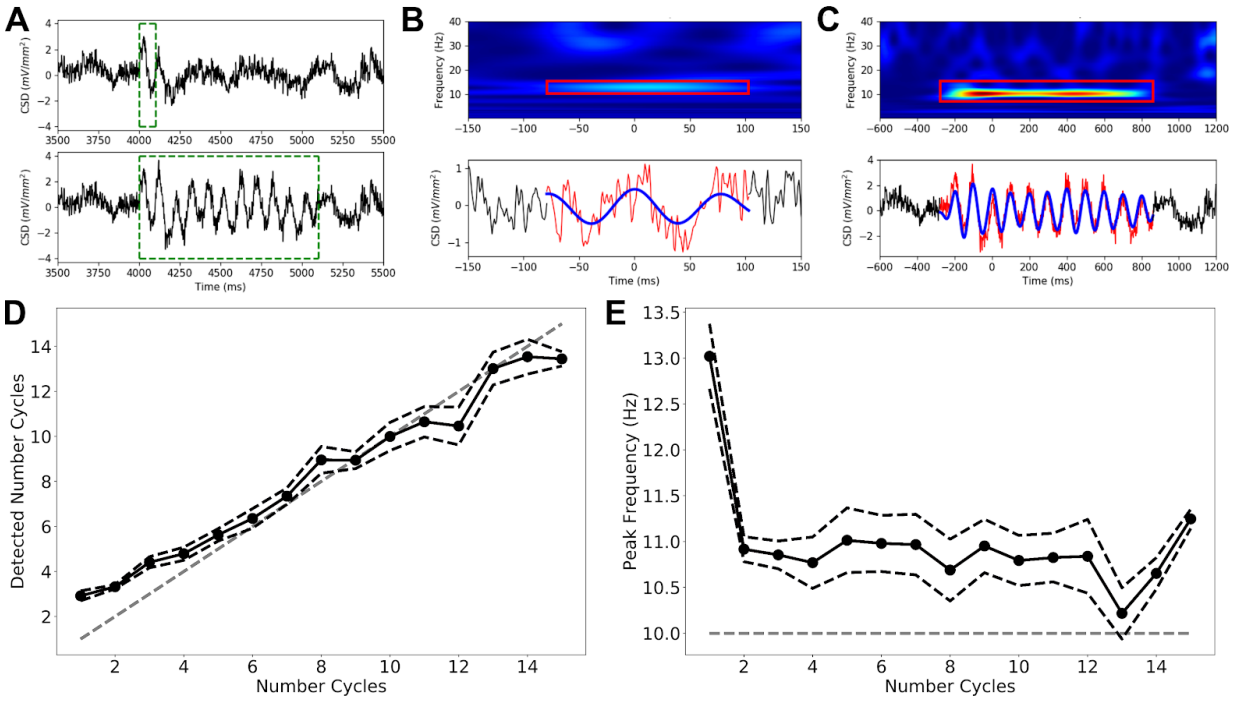

Fig. 1. Validation of event detection algorithm. (A) Example **of** 1-, 11-cycle simulated 10 Hz alpha signals (green bounding boxes) added to supragranular CSD; amplitude 1.5 mV/mm2. **(B)** 1 cycle signal from **A** was detected as 2 cycles. **(C)** 11-cycle detected as 11.7 cycles. For **B,C** Top: wavelet transform spectrograms with detected event in boxes; bottom: raw (red), filtered (blue) signal **(D)** Detected number of cycles nearly equal to actual number (dotted gray line; RMSE<1). **(E)** Peak frequency detected is generally above the frequency of the simulated 10 Hz signal (horizontal gray line). **(D,E)** (SEM: dashed lines).

Removal of externally-driven events

Event-related potentials (ERP) are prominent brief signals associated with external sensory stimuli. The wavelet transform identifies these transient signals as oscillations, obscuring our analysis. In order to remove these, we formed average ERP waveforms in supragranular, granular, and infragranular sink channels from an NHP A1 dataset, recorded during 50 dB

auditory click stimulus presentations (**Fig. 2**). The wavelet transforms of these signals showed high spectral power. Both the supragranular and infragranular ERP responses have sharp peaks that last around 50 ms, producing a 20 Hz signal in the wavelet analysis. Similarly, the granular ERP response has a slower component that lasts for approximately 100 ms, producing a 10 Hz response in the wavelet spectrogram.

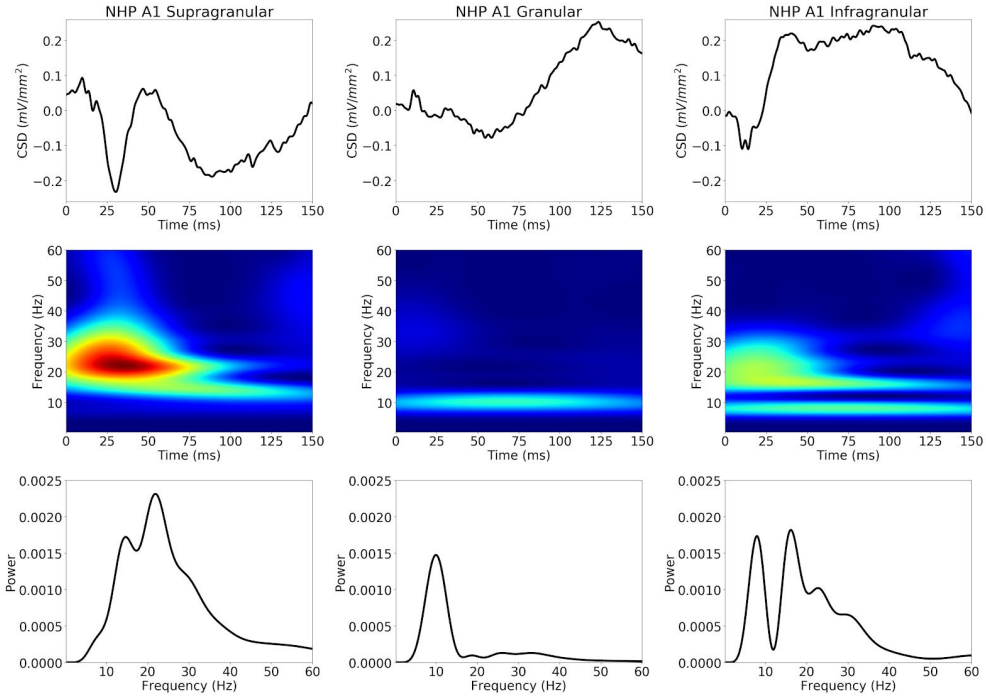

Figure 2. Stereotyped ERPs in NHP A1: supragranular, granular, infragranular layers (left to right; 50 dB clicks in NHP). Top: Average ERP waveforms (click at 0 ms). **Middle:** wavelet transform spectrograms. **Bottom:** Apparent oscillation peaks (average of spectrogram over time).

ERP score was defined as the maximum normalized cross-correlation between that event and the average ERP from the same cortical layer (**Fig 2, bottom**). An event with ERP score >0.8 with duration 75-300 ms (same range used for all layers; a loose constraint to reduce false negatives) was excluded from further analysis. ERP score was calculated for all NHP A1 events, but not for human STG where we lacked ERP data. We also excluded events with broadband frequency responses, likely from rapid-onset ERPs or recording noise. We defined logarithmic frequency span as Fspan = log(maxF/minF) using natural log, and excluded events with Fspan>1.5 (2.17 octaves).

Characterization of oscillations

8.13 hours of NHP A1 recording from 4 animals, recorded from 23-channel linear array electrodes spanning all cortical layers, were converted to current-source density (CSD) time-series to estimate neuronal ensemble transmembrane currents in specific cortical layers [15]. We analyzed over 1.9 million putative oscillation events across all recording channels after eliminating ERP-like events. We also analyzed 42 minutes of human superior temporal gyrus (STG) intracranial electroencephalogram (iEEG) recordings (5 subjects; 51,047 oscillation events). Analyses performed on the iEEG dataset used the recorded signals directly, not CSD. Re-referencing iEEG signals using a bipolar referencing scheme produced similar results. We

focused on characterization of oscillation events, as periods in the wavelet spectrogram with moderate to high power at particular frequencies (threshold of 4× median power; see **Materials and Methods**). Events were classified according to traditional bands: delta (0.5-4 Hz), theta (4-9 Hz), alpha (9-15 Hz), beta (15-29 Hz), gamma (29-80 Hz), high gamma (81-200 Hz). Event frequency was defined based on the frequency at the point of maximum power during the event.

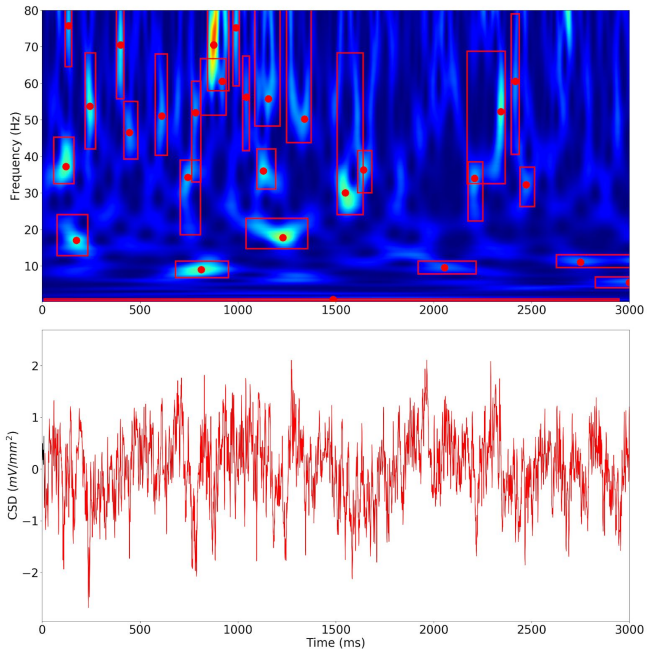

Figure 3. Events occupy the majority of recording time. Example from NHP supragranular A1. Oscillation events (red bounding boxes) occur in one or more frequency bands during this 3 s period. A long delta event is detected from t=0 to near the end of this 3 sec period (red box appears as line across bottom). Red points show peak frequency; height of box indicates frequency spread. Wavelet transform spectrogram (top) of signal shown at bottom. This example shows events in delta, theta, alpha, beta, and gamma bands.

Oscillations dominated A1 dynamics (**Fig. 3**). Oscillation events in one or more frequency bands were detectable during about 90% of total recording duration (89.1%, 89.2%, 89.6% for the 3 NHP A1 locations; 89.5% in human STG iEEG). Results were consistent across layers and between NHP and human recordings. Oscillations were typically overlapping or nested. Events varied widely in appearance, frequently with crescendo-decrescendo patterns. Many events also showed a pattern of frequency change -- up, down or U-shaped (**Fig. 4**). For example the alpha event in Fig. 4 maintained relatively constant power but first increased and then decreased in frequency, as can be seen in the time domain as well as in the spectrum. Despite the relatively broad spread of frequency, this alpha event is clearly continuous, qualifying it as a single oscillation event. The beta event in **Fig. 4** showed a different pattern: an abrupt frequency reduction concomitant with power reduction. There was also variation of frequency across events within a frequency band.

As in prior studies [4,15], delta rhythm dominated in power as well as in active time -- the **Fig. 4** delta event had 7.6× median power, with peak power at 2.5 Hz. It had 4.2 cycles, lasted 1674 ms, and had *filter-match* r=0.68 between raw and filtered waveforms. The frequency spread of this delta oscillation ranged from 1.75-3.25 Hz. Low power elsewhere in this spectrogram resulted in a high signal-to-noise ratio (SNR). Similarly, the example theta

oscillation event (**Fig. 4**, top right) had high power (6.9x median), frequency spread 3.5-5.25 Hz around peak frequency 4.25 Hz, with 5.2 cycles, and filter-match r=0.52. In both the delta and theta cases, the typical nesting of fast oscillations within the slower oscillation was seen, explaining the relatively low filter-match (see **Materials and Methods**). The **Fig. 4** alpha event had 5.9x median power with peak frequency 12.5 Hz spanning 11-19 Hz over 8.9 cycles, filter-match r=0.44. The beta event had 5.1x median power; 21 Hz peak (13.0-26.5 Hz); 7.5 cycles; r=0.54. Gamma: 6.1x; peak 46.75 Hz (36.5-61.25); 4.6 cycles; r=0.66. High gamma (HGamma): 5.2x; 147.5 Hz peak (117.75-169.25); 8.1 cycles; r=0.53.

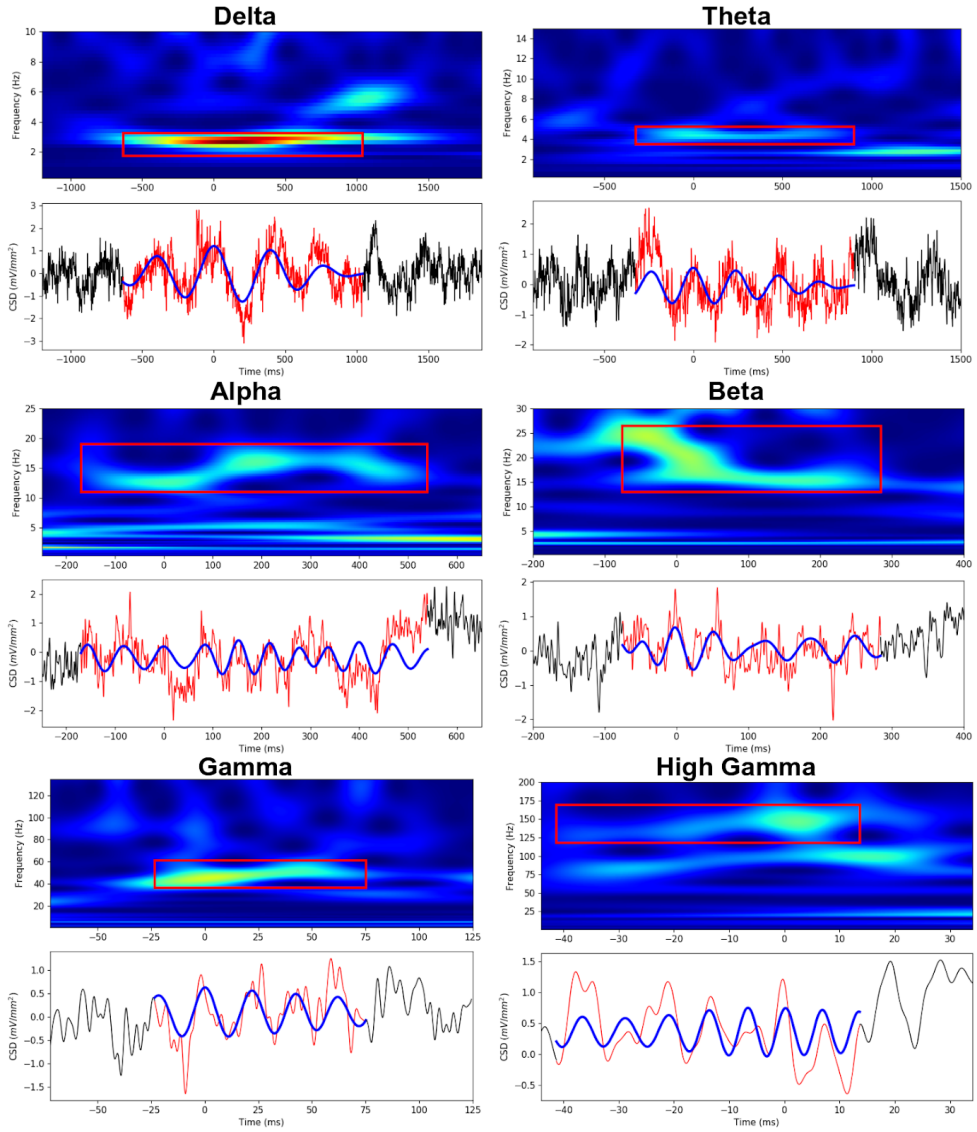

Figure 4. Oscillation events from NHP A1 supragranular layer. Morlet wavelet spectrograms demonstrating individual events (red bounding-box) with raw (red) and filtered (blue) waveforms below (black trace: period outside of detected oscillation). x- y- , and z- (color) scales differ for different bands; power range can be identified from y axis.

Given that the number of cycles was similar across oscillation frequencies, lower frequency events will necessarily occur more rarely due to their longer duration. Therefore, it was not

surprising that higher frequency events occurred most often and dominated recording time (**Fig. 5**). Longer event duration for delta oscillations produced the longest overall active time ratio (ATR -- the overall proportion of recording duration for each band) for the delta band (**Fig. 5B**). ATR values ranged from 0.19 to 0.45, with the same pattern seen in all NHP cortical layers, and in human STG: highest for delta, decreasing for theta, reaching a minimum for alpha, then increasing for beta and gamma. The ATRs add up to more than 1, greater than 100%, because of the oscillation overlap seen in **Fig 3**. Overlap was often due to nesting of a high frequency oscillation in a lower frequency event. For example, gamma and Hgamma both had high ATRs due to nesting in delta. This pattern was observed both when using longer window sizes for slower oscillation frequencies compared to faster oscillation frequencies, and when using the full recording duration for the event rate calculations.

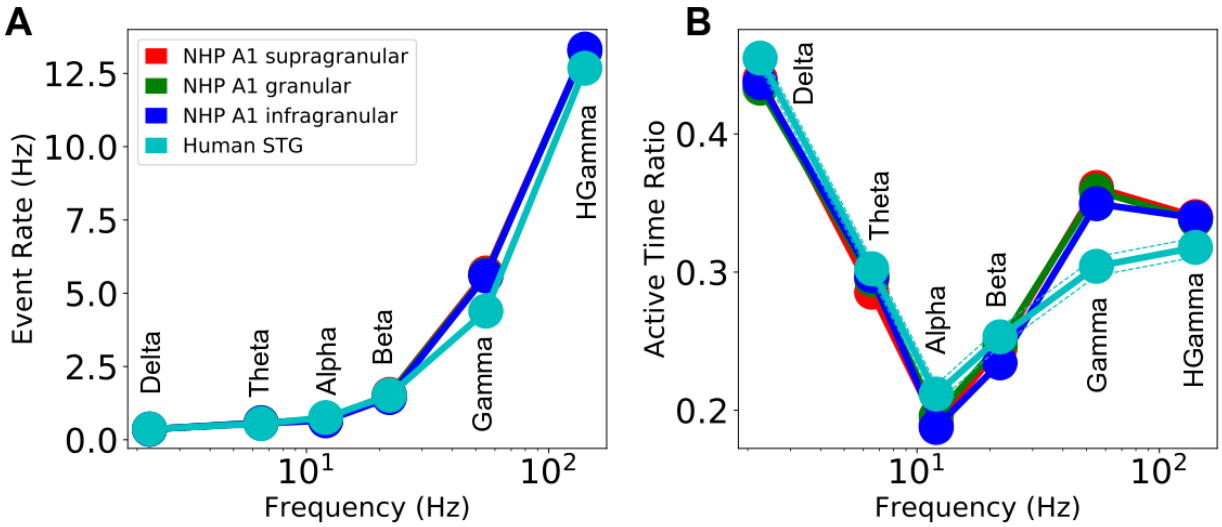

Figure 5. Oscillation event rates and active time varied by frequency band. (A) Higher frequency events are more frequent (log-log plot). (**B)** ATR: lower and higher frequency events fill much of the recording duration. (HGamma: high gamma bands; mean +/- SEM in both **A** and **B**).

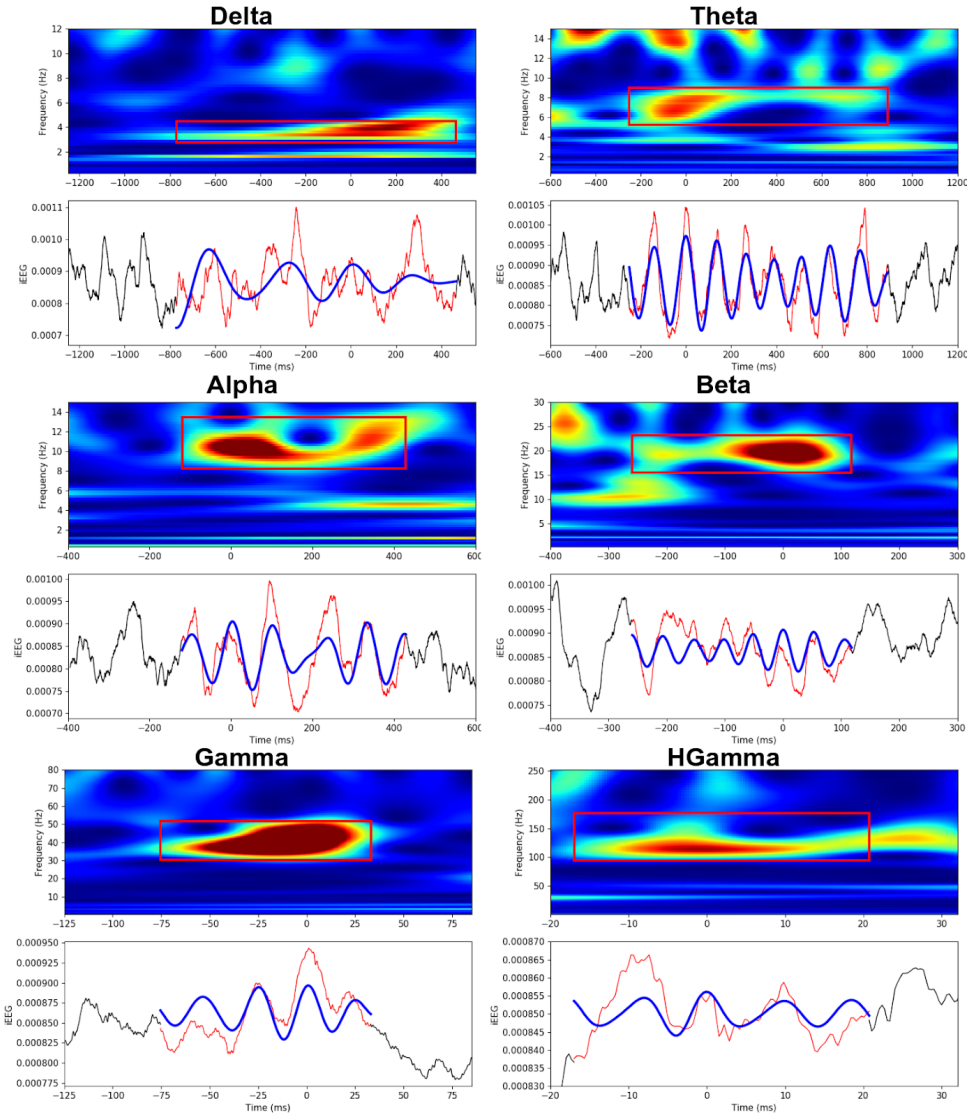

Figure 6. Oscillation events from human STG iEEG. Morlet wavelet spectrograms demonstrating individual events (red bounding-box) with raw (red) and filtered (blue) waveforms below. (x- y- , and z-(color) scales differ for different bands; power range can be identified from y axis.) Time of 0 ms corresponds to the wavelet phase of 0 radians (local maxima) closest to the event's peak power at threshold detection.

The characteristics of human oscillation events were similar to those of NHP (**Fig. 6**). Oscillation events in the human iEEG were clearly detected across all physiological oscillation bands, with multiple cycles and strong correspondence between raw and filtered waveforms. A characteristic example in each band is shown -- delta: 6.7×, 3.75 Hz (2.75-4.5), 4.6 cycles, r=0.36; theta: 5.0×, 6.5 Hz (5.25-9.0), 7.4 cycles, r=0.85; alpha: 5.9×, 10.25 Hz (8.25-13.5), 5.6 cycles, r=0.76; beta: 6.3×, 19 Hz (15.5-23.25), 7.2 cycles, r=0.59; gamma: 10.5×, 40.75 Hz (30.25-51.75), 4.4 cycles, r=0.59; high gamma: 6.3×, 114 Hz (94.5-177.25), 4.3 cycles, r=0.46. As with the NHP results, events showed intra-event shifts in frequency and amplitude, for example the alpha event in **Fig. 6** shows a central frequency dip.

Fig. 7 shows examples from NHP A1 by band, with events organized from top-to-bottom by decreasing number of cycles, and left-to-right by decreasing filter-match between their filtered and raw signals. Oscillations are easier to see in the case of high filter-match. Direct visualization of many such examples allowed us to verify that the algorithm detected reasonable-looking oscillations. The oscillations shown here had as many as 32 local peaks (**Fig. 7F,** 2 examples in green bounding box). Combinations of oscillations which co-occurred within a specific event produced differences in waveforms (*e.g,* **Fig. 7A**, green bounding box). The variability in waveform shapes and oscillation event properties suggests different circuit mechanisms for the production of individual events.

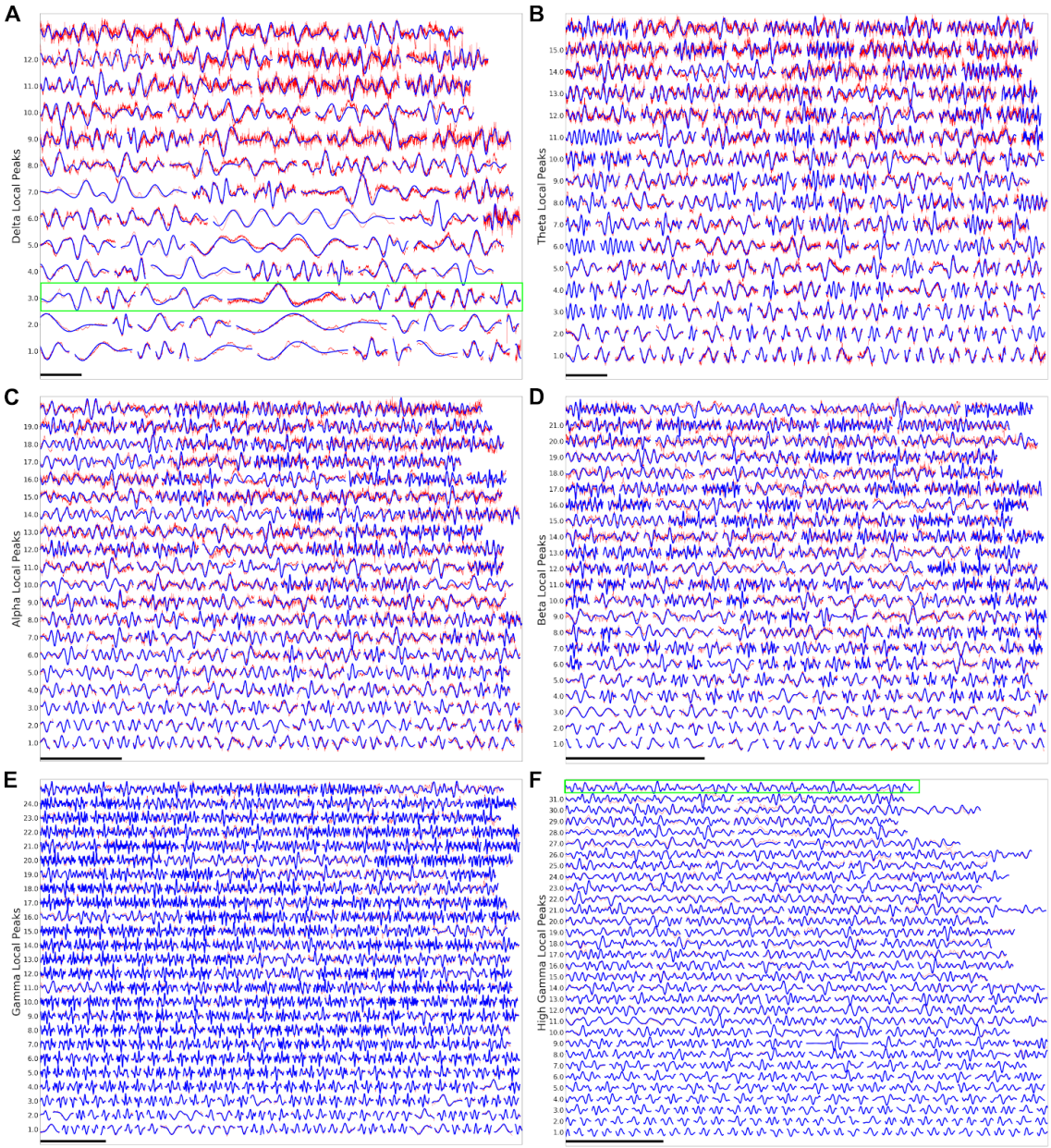

Figure 7. Individual oscillation events from NHP A1. (A) Delta, **(B)** Theta, **(C)** Alpha, **(D)** Beta, **(E)** Gamma, **(F)** High Gamma. In each case, decreasing number of cycles are shown top to bottom;

decreasing filter-match between raw and filtered from left to right. Scale bars 1 s except: E: 200 ms; F 100 ms. Examples in green bounding boxes in **(A)** and **(F)** are described in the text.

Oscillation variability

While most oscillation characteristics were consistent across NHP layer locations, they were somewhat different when compared to human recordings (**Fig. 8**; **Supporting Material Tables 2-3**). The number of detected cycles averaged 3-4 (range 1-44), increasing from delta to high gamma (**Fig. 8A**). Time-domain count of local peaks closely matched the number of calculated cycles, demonstrating the accuracy of the measures taken in the wavelet domain (**Fig. 8B**). All oscillation frequency bands above delta had numerous events with >10 cycles in both NHP and human recordings. Bandwidth was consistent across bands with intra-event Fspan showing Fmax about 65% higher than Fmin (**Fig. 8C;** antilog(0.5)=1.65). More intra-event frequency shift was seen in the delta band. Interestingly, human beta was broader in bandwidth, and human gamma tighter, compared to the values in NHP. Quality of filter-match increased with frequency in NHP (**Fig. 8D**). Filter-match was worse at the lower frequencies due to nested oscillations. This filter-match tendency differed in the human recordings, where high frequencies were poorly fitted by the filtered waveforms. This difference may be a technical consequence of volume conduction putting together iEEG sampled from many cortical layers and lateral locations, whereas NHP CSD measures were highly localized.

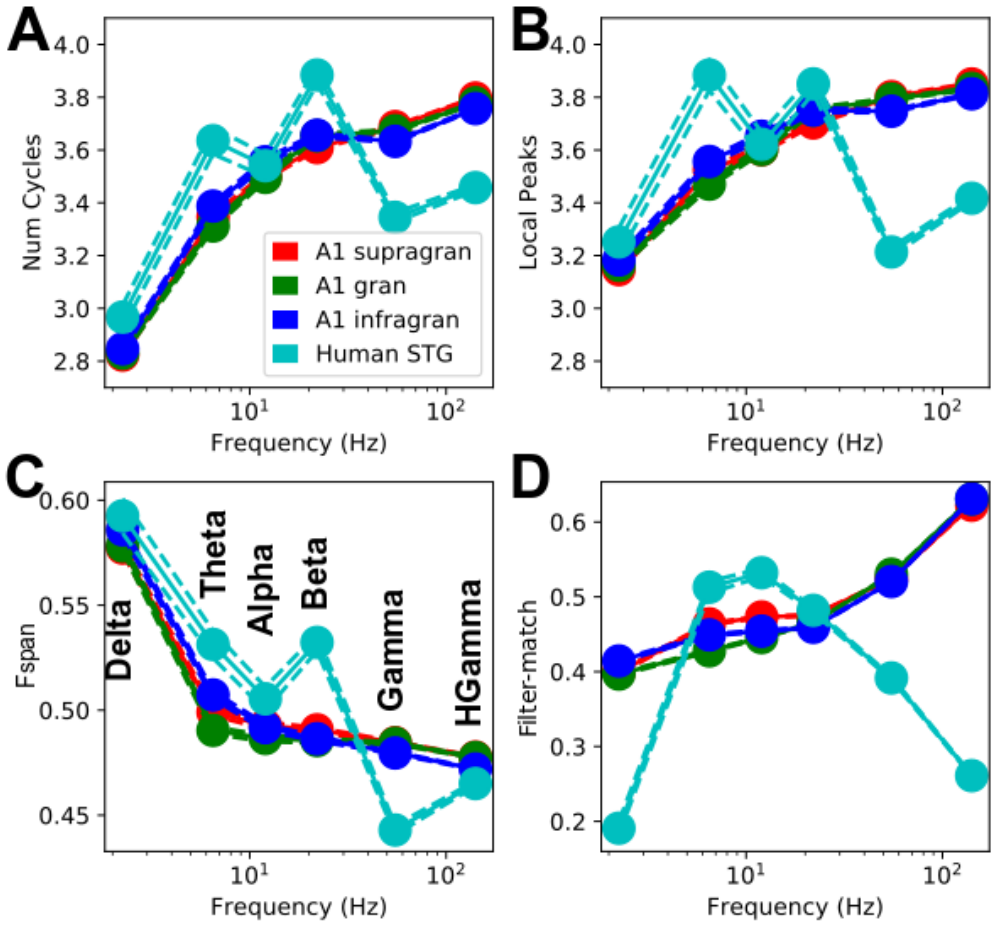

Figure 8. Event features. (A) Number of cycles. (B) Number of local peaks in time domain of filtered waveform. (C) Intra-event Fspan=log(Fmax/Fmin); 0.7 is freq doubling. (D) filter-match *r* value.

Events occurred with some degree of rhythmicity, suggesting a rhythmic occurrence of these oscillation-events within windows of time (**Fig. 9**). The testing windows of 72.0, 32.0, 25.6, 10.7, 2.8, and 1.2 s for delta, theta, alpha, beta, gamma, and high gamma were sufficient to allow about 16 events per window. Inter-event intervals within a particular band were measured as times between event peaks, or by event initiation or termination (similar results). Coefficient of variation squared (CV2) and Fano-Factor (FF) were used as tests of rhythmicity with values intermediate between 0 (fully rhythmic and predictable) and 1 (fully noisy -- Poisson distributed). Average CV2 values were all substantially lower than 1.0 (**Fig. 9A**; $p<0.05$), demonstrating that events occurred across time with some rhythmicity. FF values were also consistent with this hypothesis, with mean values lower than 1.0 (**Fig. 9B;** $p<0.05$).

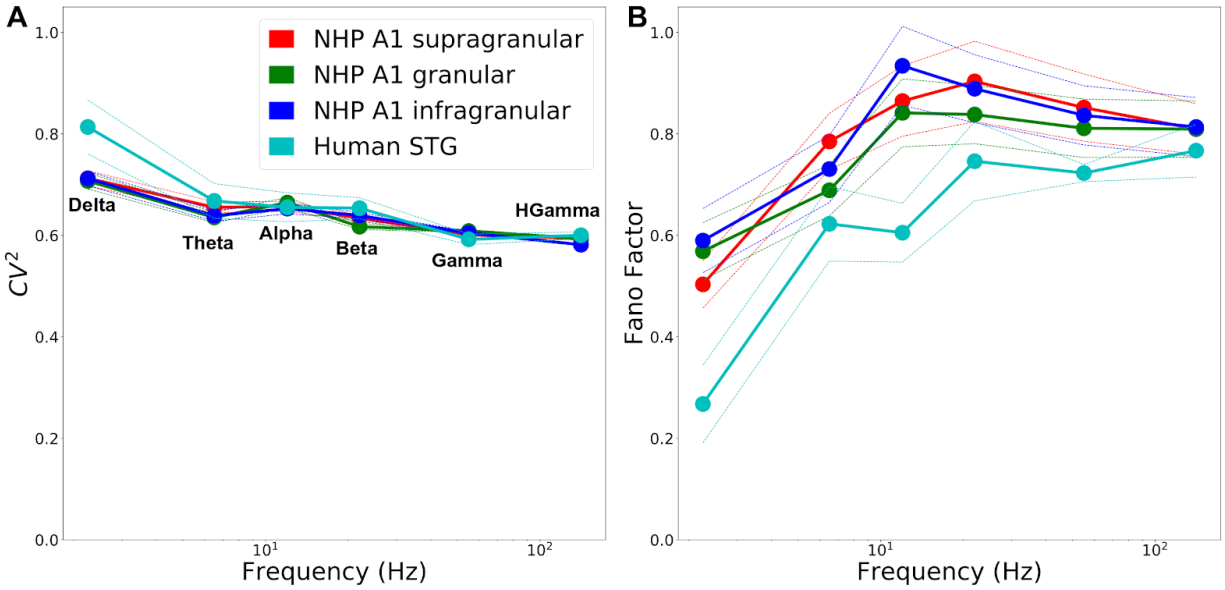

Figure 9. Inter-event intervals suggest rhythmic recurrence in all bands (A) Squared coefficient of variation CV^2. **(B)** Fano-Factor values. (mean and SEM; both cases $p<0.05$ -- one-sided Wilcoxon signed-rank test).

Discussion

We found near-continuous (90% of time) neuronal oscillations across the full range of EEG bands in a large, resting-state electrophysiology dataset invasively recorded from non-human primates and humans. Oscillations occurred in *events* of up to 44 cycles (**Fig 7F; Supporting Material Table 2**), with about 4 cycles on average (**Fig. 8A**). We developed a computational tool, *OEvent*, that used a wavelet transform to identify and characterize these events from CSD and iEEG signals, after removal of event-related potentials and broadband noise (**Fig. 2**). OEvent was validated using 10 Hz sinusoids superimposed on the fluctuating background from NHP recordings (**Fig. 1**).

We determined basic temporal features of oscillation events: power, frequency at peak power, duration, frequency spread (bandwidth), number of cycles, and filter-match (quantifies presence of pure oscillation) (**Fig. 8D**). Within-event oscillations remained within a single traditional frequency-band, but frequency was not constant within the event (*e.g.,* U-shape in **Fig. 4** alpha). Intra-event shift was on average about 65% (indicated by Fspan of ~0.5 in **Fig.**

8C). Oscillation events in a particular band occurred with some regularity, demonstrated by noting CV2 and Fano Factor values significantly less than 1. Overall, our results provide evidence that neuronal oscillations across a wide range of frequencies occur in quasi-rhythmic, multicycle events, or bursts, with significant across-burst temporal predictability. We suggest that rhythmic oscillatory bursting is the dominant operational mode of the auditory cortex in both human and non-human primates.

Oscillation event variability

Several other authors have used rigid criteria to identify oscillations, often only identifying an oscillation if it showed a single frequency, and relatively constant amplitude, across multiple cycles [25,26]. We have opted to cast our net more widely in order to capture the full variety of oscillatory phenomenology. Our main reason for this broad catchment is that we see major frequency and power shifts in a context where oscillations have a clear functional implication - for example in the delta/theta/alpha gamma modulations seen during auditory processing [27]. Strict criteria also do not adequately take into account the nonstationarity (formerly called noisiness) of brain signals due to constantly fluctuating cognitive and behavioral demands unrelated to task [28]. By taking a less restrictive approach, we discovered events with variation in cycle-to-cycle frequency and amplitude, with frequencies nonetheless remaining within the characteristic traditional frequency band.

Interpretation of rhythms, and in establishment of identities for conserved rhythmic “motifs” , relies first on measurement technology and then on methods of analysis [29]. Intracranial and extracranial recordings produce vastly different signals for interpretation that may require different tools. Even within intracranial recordings, there are important differences between depth and surface recordings, between monopolar vs bipolar recordings, and between LFP and CSD. Different frequency bands may also require different approaches, particularly in cases of unusual stereotyped events such as ripples. Different brain areas and different task conditions may also provide different signal patterns to be taken into consideration when identifying oscillation events. In the current study, we were encouraged by obtaining similar results across different measurement technologies (iEEG, LFP, CSD) and across species in resting state conditions.

In the data we analyzed, there were many intuitively clear examples of oscillations with high power, multiple cycles, relatively constrained frequency range, and sinusoidal appearance (**Fig. 4,6-7**), features typically considered when determining whether a portion of a signal contains an oscillation. Individuals will nonetheless disagree on the exact cut-offs to make this “oscillatory determination”. This subjectivity makes it difficult for the community to arrive at a consensus on the importance of oscillations in the brain. A further complication is that data used in publications is rarely presented in “raw form.” We have therefore presented a heterogeneous portion of the dataset used in the Results in **Fig. 7**, to allow readers to view examples of oscillations with all of their variability.

The contrast between our identification of high oscillation variability with a more rigid interpretation of oscillation identity can be seen by comparing our techniques with those of Voytek and colleagues [25], which only considered oscillations with consistent features over time. Their method first performed low-pass filtering to remove high-frequency noise, followed by band-pass filtering to narrow-in on a frequency of interest. Next, their algorithm extracted

local minima/maxima of individual cycles in the filtered time-domain signal, and analyzed cycle-by-cycle properties, checking for consistency of features over time [19,25]. Voytek's algorithm thereby provided criteria for defining stationary neural oscillations by assuming consistency of cycle-to-cycle amplitude and frequency during the single event. The algorithm also used a minimum threshold for the number of cycles in an oscillation. While this approach is very useful, we argue that at first, we should detect all potential oscillatory events, extract their basic properties, and then clearly state which properties identify actual oscillation events. Of course these criteria will be somewhat subjective, but at least they are clearcut, which will make any oscillation based results more replicable.

In the future, collaborative software tools and additional data sharing will improve consistency in the research community and make faster progress. To this end, we are sharing the current datasets. Researchers can use our datasets and accompanying OEvent tool (https://github.com/NathanKlineInstitute/OEvent) to rate rhythmicity within and among events, to evaluate and compare event detection tools, and to develop new tools. Further progress would come from embedding software platforms in web front-ends to allow researchers to view neurophysiological data and perform oscillation scoring on signals in public datasets or from their own data. This process would help the community come to a consensus on neurophysiological oscillations and the features that contribute to oscillations *vs.* event-like waveforms, as well as objectively defining rhythmicity using measures such as coefficient of variation squared (CV2), Fano Factor, or a modified version of lagged coherence that operates on events [30]. Consistent consensus across studies may be somewhat limited by different signal patterns in different brain areas or under different task conditions.

Other published methods have analyzed signals in only the frequency domain [31] or in only the time domain [32]. As shown in the present paper, there are clear advantages in moving back and forth across these different views into dynamics. Here, we were able to more accurately exclude ERPs using features from both domains: *e.g.,* waveform shape and duration (time-domain), along with frequency-span (frequency-domain). Our analysis on the quasi-rhythmicity of oscillation events relied on first defining the events using the frequency domain (wavelet transform) and then using time-domain to measure inter-event rhythmicity (CV2 of interevent intervals).

In future work, we will look for signatures or motifs of particular oscillation types at particular depth locations. This will consist of looking at patterns of crescendos and decrescendos in activation power, or patterns of increases and decreases in frequency. For example in the Fig. 4 alpha trace, the wavelet pattern shows a rapid increase in power and then gradual decrease, while the frequency goes first down and then up.

Mechanisms of oscillation generation

Biophysical computer modeling of detailed microcircuits can also help define oscillations and their properties, by allowing predictions about the mechanistic origins and temporal fluctuations of specific oscillation types and their recurrence over time [33,34], and how different oscillation generators interact [24,35–38].

Detailed computational modeling of neural circuits has shown how interactions between different classes of interneurons contribute to fast and slow rhythms, via short and long $GABA_A$

synaptic time constants [39–42]. *In vivo*, we expect that interactions between different interneuron sub-populations and pyramidal neurons will result in a mix of oscillations in the recorded signals [43–47], making it unlikely to observe a constant frequency/amplitude oscillation. Some of these interactions, which could lead to shifts in peak oscillation frequency over time or variability in waveform shapes in different nearly simultaneous oscillation events, could be explored through detailed computational modeling. In addition, differences in recording methods (electrode properties and volume recorded from) between NHP and humans could be investigated with detailed biophysical modeling.

Data-driven modeling could also pave the way for understanding the extent to which electrophysiological measurements are contaminated by noise, and which type of waveforms one can expect to see in electrophysiological signals recorded during different experimental conditions. Biophysical modeling could further allow us to develop a revised taxonomy of the different oscillations, by predicting which circuit components each oscillation arises from. A clearer understanding of the mechanisms creating oscillations will pave the way to improving neuropathologies associated with disrupted brain rhythms, via pharmacology or targeted neuromodulation that normalizes rhythmic activity in a principled manner.

Ubiquity of oscillatory events

To our knowledge, our is the first study to systematically quantify the full range of physiological oscillations in the auditory cortex, using the novel method of oscillation event analysis. Prior studies have shown that high-power beta rhythms emerge as brief transient events lasting only a few cycles, in somatosensory [20,23], motor [48–50] and frontal cortex [20,51]. In somatosensory cortex, extracranial measurement in humans, and intracranial in mice and NHP [20,23] showed a low rate of beta events comparable to what we observed (1.4-1.6 Hz; **Supporting Material Table 1A**). We found 3.6-3.9 cycles per event (**Supporting Material Table 2**) somewhat higher than the less than three cycles found in the prior studies. Our merging of events when bounding boxes overlapped by 50%, could produce our somewhat larger number of cycles. In addition, in our present study we used a lower threshold (4x median compared to the 6x median threshold used previously), and thereby potentially allowed detection of a larger set of oscillation events with different properties. Further research is required to determine if there are more similarities between beta bursts in the auditory cortex as compared to other brain areas and studies.

Consistent with our analyses, a study recording electrophysiology data from cat auditory cortex demonstrated that gamma rhythms are non-stationary, and event-like [21]. The study also found that gamma events' peak frequency was dependent on arousal level, while amplitude was more dependent on attention. This, and our current results highlight the importance of characterizing multiple "oscillatory dimensions", in order to better understand how oscillatory features relate to brain function. Other studies show that both beta and gamma bursts contribute to working memory processes [22]. Although these studies did not specifically quantify predictability of gamma recurrence over time during spontaneous activity, related evidence from the auditory cortex [52] and other brain areas [53] shows that the phase of low-frequency rhythms (delta/theta/alpha) influences the amplitude of higher-frequency rhythms (beta, gamma) in a predictable way, which is termed phase amplitude coupling [54–56]. Other recent studies show that apart from predictability in time, there is predictability in the spatial location where gamma

bursts occur: precisely orchestrated alpha waves traveling over the cortical surface regulate the timing of bursts of localized gamma activity [57].

Functional implications

Although our study was specifically designed to be non-task-related, no effort was made to make the subjects cognitively or perceptually inactive. Although the term *resting-state* is applied to this condition, the brain is never functionally at rest [28] as it would be in sleep or anesthesia. The brain activity we have measured is that of a perceiving, thinking brain -- hence we prefer *non-task-related state* to *resting state*.

Oscillations are sometimes considered to be functionally irrelevant, epiphenomenological. By contrast, we and others view oscillations as fundamental to brain function and brain encodings, and view understanding the roles of oscillations as being critical for understanding the brain [58]. In a trivial sense, oscillations are epiphenomena since they reflect an electric field that is only an external reflection of internal dynamics; in this same sense an external recording of an action potential is an epiphenomenon. The important question is whether aspects of the oscillation, or aspects of a single-neuron spike train or aspects of oxygenation state in a brain area, can be regarded as having a role in coding and representations [59,60]. The notion of coding itself then breaks into 2 meanings: correlative coding that can be observed by the experimenter vs. causal, internal coding that forms part of how the animal behaves or thinks. Correlative coding is more studied; causal coding is more important.

As with the single-neuron firing-rate causal coding hypothesis, evidence for oscillation causal coding is inferential and hypothetical. The major hypotheses on the role of oscillations are entrainment theory [4–6] and communication through coherence theory [8,11]. Grossly, both of these theories consider the role of phase synchronization in gating communication channels across brain circuits. Specific frequency bands have been implicated in particular aspects of neural state: attention indexing by alpha in auditory, visual and somatosensory areas [14,15,61,62]; stimulus timing by aligned delta-theta [63,64]; delta with nested gamma by encoding of elements of speech signals [27,65,66]. The present study demonstrates that oscillations are ubiquitous across bands and thus would provide fertile ground for their use in these contexts. At a fundamental level, the oscillations we observed reflect ensembles of neurons activated synchronously and projecting activity together both within and between areas.

An additional hypothesized oscillation role involves the control and molding of higher frequency oscillation nested within lower. Evidence for such frequency nesting was seen by our filter-match measure (Fig 8D), which measured the difference between a clean, but not necessarily single frequency, sinusoid and the recorded wave. Further work remains to be done in determining the ranges and relations of particular nested frequencies relative to particular nesting frequency. We also observed another indication of oscillation variability, the ~65% variation in frequency of a primary oscillation, demonstrated by the Fspan measure in many events (Fig 8C). Both nested oscillations and oscillation frequency-spread could be features of entrainment theory and communication through coherence. Alternatively, one or both of these might be an indicator of an underlying embedded encoding.

Materials and Methods

Datasets

We used two datasets of neuronal activity, invasively recorded over longer time scales (minutes) in non-task related conditions: 1) laminar electrode array local field potentials from non-human primate (NHP) primary auditory cortex (A1; 92 recordings totaling 487.8 minutes); 2) intracranial EEG (iEEG) from human superior temporal gyrus (STG; 9 recordings totaling 42 minutes).

1) NHP electrophysiological data was recorded during acute penetrations of area A1 of the auditory cortex of 1 male and 3 female rhesus macaques weighing 5-8 kg, who had been prepared surgically for chronic awake electrophysiological recordings. Prior to surgery, each animal was adapted to a custom fitted primate chair and to the recording chamber. All procedures were approved in advance by the Animal Care and Use Committee of the Nathan Kline Institute. The data were recorded during waking rest with eyes mostly open.

2) The iEEG data was recorded at Northshore University Hospital in medically-intractable epilepsy patients that underwent stereotactic depth electrode placement as part of their epilepsy surgery workup. Electrode placement was based on clinical criteria only. All patients provided written informed consent monitored by the institutional review board at the Feinstein Institutes for Medical Research. Electrode localization methods have been described previously [67]. The data was recorded using a Tucker Davis Technologies amplifier with a sampling rate of 3000Hz. The data were recorded during waking rest with eyes closed.

Data processing

All analyses from the NHP dataset were run on current-source density signals, calculated as the second spatial derivative of laminar local field potential recordings . To reduce computation time, we only used channels that included the supragranular, granular, and infra-granular current sinks in response to preferred frequency tones, considered “active” since they measure depolarizing transmembrane currents [15]. All analyses from the iEEG dataset used the recorded signals themselves without taking any spatial derivative (re-referencing signals using a bipolar reference produced similar results; not shown).

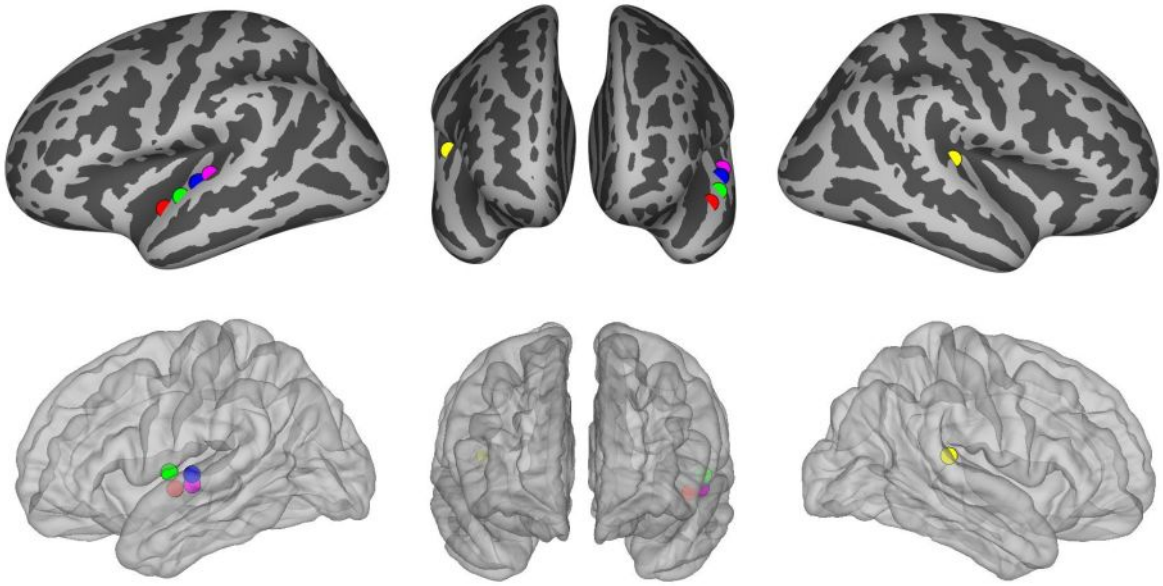

Figure 10. Locations of the intracranial EEG electrodes used for human electrophysiology recordings included in this study, overlayed on a standard average brain. Colors represent different patients.

Oscillation event detection and feature extraction

We extracted moderate/high-power spectral events using 7-cycle Morlet wavelets on non-overlapping 10 s windows [20,38]. The 7-cycle Morlet wavelets were chosen to provide an adequate compromise between time and frequency resolution [17]. We used linearly spaced frequencies (0.25 Hz frequency increments), ranging from 0.25 - 250 Hz, to compute the wavelets. The power time-series of each wavelet transform was normalized by median power across the full recording duration. We then applied a local maximum filter to detect peaks in the wavelet transform spectrogram. All local peaks were assessed to determine whether their power value exceeded a threshold. We used a moderate power threshold (4× median) to determine the occurrence of moderate- to high-power events.

A local power peak in the spectrogram was defined within the local 3x3 window it was centered in, and exceeded the 4× median threshold of each individual frequency. The frequency and time bounds around that peak were determined by including time and frequency values before/after and above/below the peak frequency until the power value fell below the smaller of ½ maximum event amplitude and 4× median threshold. As shown in **Fig. 3**, this produces a bounding box around each oscillation event that can be used to determine frequency spread (minF to maxF), time span (start, stop), and peak frequency (defined as the frequency at which maximum wavelet power is detected). After the initial set of oscillation events is detected, we merge events when their bounding box overlapping area in the wavelet spectrogram exceeds 50% of the minimum area of each individual event. This allows continuity of events that are separated by minor fluctuations below threshold.

We then calculated additional features from this set of events. We calculated the number of cycles by multiplying the event duration by its peak frequency. We also filtered the underlying signals of each event using a zero-phase shift bandpass filter within the minF and maxF

frequency ranges, defined on a per-event basis (as in bounding boxes shown in **Fig. 3**). We calculated filter-match value *r*, defined as the Pearson correlation between this filtered signal and the raw signal, and used it as an index of how clearly the event oscillation is visible in the raw signal. Based on visual inspection of numerous waveforms, we suggest associating the following ranges of filter-match values with the corresponding qualitative assessments (0.0-0.25:weak; 0.25-0.5:moderate; >0.5:strong/high). Using the filtered signal also allowed us to count other features of the oscillation, including number of peaks (local maxima) and number of troughs (local minima). Number of peaks and the number of cycles were highly correlated. In figures showing waveforms of individual events, the 0 time alignment is taken as the wavelet transform 0 phase closest to the time of event threshold.

After extracting individual oscillation events, we classified them into the standard physiological oscillation frequency bands on the following intervals: delta (0.5-4 Hz), theta (4-9 Hz), alpha (9-15 Hz), beta (15-29 Hz), gamma (29-80 Hz), high gamma (81-200 Hz). This classification was based on the frequency at which maximum power occurred during each event (intervals were open on the lower bound and closed on the upper bound).

Inter-event interval characterization

To measure rhythmicity across events from a given oscillation frequency band, we formed inter-event interval (IEI) distributions from the oscillation events which were not characterized as ERPs (see **Results**). We formed the intervals in two ways: 1) the interval between the time of peak power of the previous event to the time of peak power of the next event; 2) the interval between the end of the previous event to the start of the next event. After forming IEI distributions, we calculated its squared coefficient of variation (CV2). We also calculated the Fano Factor (FF) from the number of events in successive windows (defined below). A Poisson distribution will have CV2 and FF values of 1, while more rhythmic processes have CV2 < 1, while more “bursty” processes (multiple characteristic inter-event intervals) will have CV2 > 1. CV2 values increased with the number of events in a time window, for both longer windows of analysis and higher frequency oscillations. To control for this, we varied window size for different frequencies (longer for slower frequencies) to produce a similar number of events per window (N=16). The empirically-determined window sizes used were 72.0, 32.0, 25.6, 10.7, 2.8, and 1.2 s for delta, theta, alpha, beta, gamma, and high gamma frequency oscillations, respectively. We used a one-sided Wilcoxon signed-rank test to determine that the measured average CV2 and FF values were lower than those of a Poisson process.

Source code

Python source code for our OEvent software package, for oscillation event detection and analysis is available on github at https://github.com/NathanKlineInstitute/OEvent

Acknowledgments

Research supported by NIH R01DC012947, Army Research Office W911NF-19-1-0402, New York State ECRIP Fellowship, NIH P50 MH109429, NIH R01MH106174, NIH U24EB028998, NIH U01EB017695, NYS SCIRB DOH01-C32250GG- 3450000, NSF 1904444.

Supporting Material

Event Rate	Delta	Theta	Alpha	Beta	Gamma	High Gamma
A1 Supra	0.36+/-0.0 (10,611)	0.57+/-0.0 (16,602)	0.67+/-0.01 (19,587)	1.55+/-0.01 (45,258)	5.69+/-0.01 (166,532)	13.28+/-0.02 (388,744)
A1 Gran	0.36+/-0.0 (10,537)	0.58+/-0.0 (17,081)	0.69+/-0.0 (20,138)	1.52+/-0.01 (44,622)	5.63+/-0.01 (164,729)	13.25+/-0.02 (387,752)
A1 Infra	0.36+/-0.0 (10,578)	0.57+/-0.0 (16,840)	0.65+/-0.01 (18,978)	1.44+/-0.01 (42,229)	5.59+/-0.01 (163,555)	13.33+/-0.02 (390,097)
STG	0.37+/-0.01 (941)	0.55+/-0.01 (1,388)	0.76+/-0.02 (1,901)	1.52+/-0.02 (3,828)	4.39+/-0.05 (11,069)	12.68+/-0.07 (31,920)

Supporting Table 1A. Average Event Rate (Hz) +/- standard error of the mean, and event count in parentheses, for the different physiological oscillation frequency bands. A1 Supra, A1 Gran, A1 Infra are from NHP A1 supragranular, granular, and infragranular sink channels, respectively. STG is from human iEEG recorded in supratemporal gyrus.

ATR	Delta	Theta	Alpha	Beta	Gamma	High Gamma
A1 Supra	0.44	0.29	0.19	0.25	0.36	0.34
A1 Gran	0.43	0.29	0.20	0.25	0.36	0.34
A1 Infra	0.44	0.30	0.19	0.23	0.35	0.34
STG	0.45	0.30	0.21	0.25	0.30	0.32

Supporting Table 1B. Active time ratio (ATR) for the different physiological oscillation frequency bands. Mean value is presented (standard error was negligible). A1 Supra, A1 Gran, A1 Infra are from NHP A1 supragranular, granular, and infragranular sink channels, respectively. STG is from human iEEG recorded in supratemporal gyrus.

Supporting Tables 2-3 list ranges and mean+/-standard error of the mean.

Cycles Per Event	Delta	Theta	Alpha	Beta	Gamma	High Gamma
A1 Supra	0.4-12.4; 2.8+/-0.0	0.7-17.2; 3.3+/-0.0	1.1-21.1; 3.5+/-0.0	1.1-23.5; 3.6+/-0.0	0.7-30.4; 3.7+/-0.0	0.6-37.8; 3.8+/-0.0
A1 Gran	0.5-11.1; 2.8+/-0.0	0.7-18.9; 3.3+/-0.0	0.7-19.6; 3.5+/-0.0	0.8-31.4; 3.7+/-0.0	0.6-30.0; 3.7+/-0.0	0.5-44.2; 3.8+/-0.0
A1 Infra	0.3-13.1; 2.8+/-0.0	0.9-18.6; 3.4+/-0.0	0.7-27.9; 3.6+/-0.0	0.6-21.8; 3.7+/-0.0	0.5-30.0; 3.6+/-0.0	0.5-34.9; 3.8+/-0.0
STG	0.5-7.0; 3.2+/-0.3	1.7-13.4; 4.0+/-0.4	1.8-19.1; 3.9+/-0.3	1.9-9.8; 3.9+/-0.1	1.5-16.0; 3.8+/-0.1	1.0-23.2; 3.3+/-0.1

Supporting Table 2. Cycles Per Event for the different physiological oscillation frequency bands. Range and mean+/-standard error of the mean, separated by semicolon (;). A1 Supra, A1 Gran, A1 Infra are from NHP A1 supragranular, granular, and infragranular sink channels, respectively. STG is human iEEG signals recorded from supratemporal gyrus.

Local Peaks	Delta	Theta	Alpha	Beta	Gamma	High Gamma
A1 Supra	0-3; 3.1+/-0.0	1-19 3.5+/-0.0	1-22; 3.6+/-0.0	0-28; 3.7+/-0.0	0-42; 3.8+/-0.0	0-36; 3.9+/-0.0
A1 Gran	0-16; 3.2+/-0.0	1-26; 3.5+/-0.0	0-26; 3.6+/-0.0	0-30; 3.8+/-0.0	0-32; 3.8+/-0.0	0-40; 3.8+/-0.0
A1 Infra	0-16; 3.2+/-0.0	0-26; 3.6+/-0.0	0-22; 3.7+/-0.0	0-31; 3.8+/-0.0	0-46; 3.7+/-0.0	0-35; 3.8+/-0.0
STG	0-8; 3.5+/-0.3	2-15; 4.5+/-0.4	1-16; 4.0+/-0.3	2-11; 3.7+/-0.1	1-20; 3.6+/-0.1	1-19; 3.1+/-0.1

Supporting Table 3. Number of local peaks in filtered waveforms for the different physiological oscillation frequency bands. Range and mean+/-standard error of the mean are presented, separated by semicolon (;). A1 Supra, A1 Gran, A1 Infra are from NHP A1 supragranular, granular, and infragranular sink channels, respectively. STG is human iEEG signals recorded from supratemporal gyrus.

Fspan	Delta	Theta	Alpha	Beta	Gamma	High Gamma
A1 Supra	0.577+/-0.002	0.499+/-0.002	0.493+/-0.002	0.491+/-0.001	0.485+/-0.001	0.478+/-0.0
A1 Gran	0.578+/-0.002	0.490+ 0.002	0.489+/-0.002	0.486+/-0.001	0.484+/-0.001	0.477+/-0.0
A1 Infra	0.586+/-0.002	0.507+/-0.002	0.492+/-0.002	0.486+/-0.001	0.480+/-0.001	0.472+/-0.0
STG	0.593+/-0.008	0.531+/-0.006	0.505+/-0.006	0.532+/-0.004	0.443+/-0.002	0.465+/-0.001

Supporting Table 4. Logarithmic frequency bandwidth (Fspan) for the different physiological oscillation frequency bands. Values are mean+/-standard error of the mean. A1 Supra, A1 Gran, A1 Infra are from NHP A1 supragranular, granular, and infragranular sink channels, respectively. STG is human iEEG signals recorded from supratemporal gyrus.

Filter-match	Delta	Theta	Alpha	Beta	Gamma	High Gamma
A1 Supra	0.399+/-0.002	0.464+/-0.001	0.473+/-0.001	0.475+/-0.001	0.524+/-0.000	0.622+/-0.000
A1 Gran	0.397+/-0.002	0.428+/-0.001	0.446+/-0.001	0.465+/-0.001	0.530+/-0.000	0.631+/-0.000
A1 Infra	0.414+/-0.002	0.449+/-0.001	0.454+/-0.001	0.459+/-0.001	0.520+/-0.000	0.631+/-0.000
STG	0.191+/-0.009	0.513+/-0.008	0.532+/-0.005	0.482+/-0.003	0.392+/-0.002	0.261+/-0.001

Supporting Table 5. Correlation between filtered and raw signals (Filter-match) for the different physiological oscillation frequency bands. Values are mean+/-standard error of the mean. A1 Supra, A1 Gran, A1 Infra are from NHP A1 supragranular, granular, and infragranular sink channels, respectively. STG is human iEEG signals recorded from supratemporal gyrus.

References

1. Obleser J, Henry MJ, Lakatos P. What do we talk about when we talk about rhythm? PLoS Biol. 2017;15: e2002794.

2. Jones SR. When brain rhythms aren't "rhythmic": implication for their mechanisms and meaning. Curr Opin Neurobiol. 2016;40: 72–80.

3. Buzsáki G, Draguhn A. Neuronal oscillations in cortical networks. Science. 2004;304: 1926–1929.

4. Lakatos P, Karmos G, Mehta AD, Ulbert I, Schroeder CE. Entrainment of neuronal oscillations as a mechanism of attentional selection. Science. 2008;320: 110–113.

5. Lakatos P, Gross J, Thut G. A New Unifying Account of the Roles of Neuronal Entrainment. Curr Biol. 2019;29: R890–R905.

6. Barczak A, O'Connell MN, McGinnis T, Ross D, Mowery T, Falchier A, et al. Top-down, contextual entrainment of neuronal oscillations in the auditory thalamocortical circuit. Proc Natl Acad Sci U S A. 2018;115: E7605–E7614.

7. Barczak A, Haegens S, Ross DA, McGinnis T, Lakatos P, Schroeder CE. Dynamic Modulation of Cortical Excitability during Visual Active Sensing. Cell Rep. 2019;27: 3447–3459.e3.

8. Fries P. Rhythms for Cognition: Communication through Coherence. Neuron. 2015;88: 220–235.

9. Fries P, Reynolds JH, Rorie AE, Desimone R. Modulation of oscillatory neuronal synchronization by selective visual attention. Science. 2001;291: 1560–1563.

10. Schoffelen J-M, Poort J, Oostenveld R, Fries P. Selective movement preparation is subserved by selective increases in corticomuscular gamma-band coherence. J Neurosci. 2011;31: 6750–6758.

11. Fries P. Neuronal gamma-band synchronization as a fundamental process in cortical computation. Annu Rev Neurosci. 2009;32: 209–224.

12. Buzsáki G. Theta oscillations in the hippocampus. Neuron. 2002;33: 325–340.

13. Lopes Da Silva FH, Storm Van Leeuwen W. The cortical source of the alpha rhythm. Neurosci Lett. 1977;6: 237–241.

14. Haegens S, Barczak A, Musacchia G, Lipton ML, Mehta AD, Lakatos P, et al. Laminar Profile and Physiology of the α Rhythm in Primary Visual, Auditory, and Somatosensory Regions of Neocortex. J Neurosci. 2015;35: 14341–14352.

15. Lakatos P, Barczak A, Neymotin SA, McGinnis T, Ross D, Javitt DC, et al. Global dynamics

of selective attention and its lapses in primary auditory cortex. Nat Neurosci. 2016. doi:10.1038/nn.4386

16. Thies M, Zrenner C, Ziemann U, Bergmann TO. Sensorimotor mu-alpha power is positively related to corticospinal excitability. Brain Stimul. 2018;11: 1119–1122.

17. Jones SR, Pritchett DL, Sikora MA, Stufflebeam SM, Hämäläinen M, Moore CI. Quantitative analysis and biophysically realistic neural modeling of the MEG mu rhythm: rhythmogenesis and modulation of sensory-evoked responses. J Neurophysiol. 2009;102: 3554–3572.

18. Halgren M, Ulbert I, Bastuji H, Fabó D, Erőss L, Rey M, et al. The generation and propagation of the human alpha rhythm. Proc Natl Acad Sci U S A. 2019;116: 23772–23782.

19. Cole SR, Voytek B. Brain Oscillations and the Importance of Waveform Shape. Trends Cogn Sci. 2017;21: 137–149.

20. Sherman MA, Lee S, Law R, Haegens S, Thorn CA, Hämäläinen MS, et al. Neural mechanisms of transient neocortical beta rhythms: Converging evidence from humans, computational modeling, monkeys, and mice. Proc Natl Acad Sci U S A. 2016;113: E4885–94.

21. Lakatos P, Szilágyi N, Pincze Z, Rajkai C, Ulbert I, Karmos G. Attention and arousal related modulation of spontaneous gamma-activity in the auditory cortex of the cat. Brain Res Cogn Brain Res. 2004;19: 1–9.

22. Lundqvist M, Rose J, Herman P, Brincat SL, Buschman TJ, Miller EK. Gamma and Beta Bursts Underlie Working Memory. Neuron. 2016;90: 152–164.

23. Shin H, Law R, Tsutsui S, Moore CI, Jones SR. The rate of transient beta frequency events predicts behavior across tasks and species. Elife. 2017;6. doi:10.7554/eLife.29086

24. Law RG, Pugliese S, Shin H, Sliva D, Lee S, Neymotin S, et al. A supragranular nexus for the effects of neocortical beta events on human tactile perception. bioRxiv. 2019. p. 750992. doi:10.1101/750992

25. Cole S, Voytek B. Cycle-by-cycle analysis of neural oscillations. doi:10.1101/302000

26. Haller M, Donoghue T, Peterson E, Varma P, Sebastian P, Gao R, et al. Parameterizing neural power spectra. bioRxiv. 2018. p. 299859. doi:10.1101/299859

27. Giraud A-L, Poeppel D. Cortical oscillations and speech processing: emerging computational principles and operations. Nat Neurosci. 2012;15: 511–517.

28. Musall S, Kaufman MT, Juavinett AL, Gluf S, Churchland AK. Single-trial neural dynamics are dominated by richly varied movements. Nat Neurosci. 2019;22: 1677–1686.

29. de Cheveigné A, Nelken I. Filters: when, why, and how (not) to use them. Neuron. 2019. Available: https://www.sciencedirect.com/science/article/pii/S0896627319301746

30. Fransen AMM, van Ede F, Maris E. Identifying neuronal oscillations using rhythmicity.

Neuroimage. 2015;118: 256–267.

31. Voytek B, Kramer MA, Case J, Lepage KQ, Tempesta ZR, Knight RT, et al. Age-Related Changes in 1/f Neural Electrophysiological Noise. J Neurosci. 2015;35: 13257–13265.

32. Neymotin S, Uhlrich DJ, Manning KA. Data-mining of time-domain features from neural extracellular field data. in Biomedicine and …. 2008. Available: https://link.springer.com/chapter/10.1007/978-3-540-70778-3_5

33. Neymotin SA, Talbot ZN, Jung JQ, Fenton AA, Lytton WW. Tracking recurrence of correlation structure in neuronal recordings. J Neurosci Methods. 2017;275: 1–9.

34. Neymotin SA, Lee H, Fenton AA, Lytton WW. Interictal EEG Discoordination in a Rat Seizure Model. J Clin Neurophysiol. 2010;27: 438.

35. Neymotin SA, Lee H, Park E, Fenton AA, Lytton WW. Emergence of physiological oscillation frequencies in a computer model of neocortex. Front Comput Neurosci. 2011;5: 19.

36. Dura-Bernal S, Neymotin SA, Suter BA, Shepherd GMG, Lytton WW. Multiscale dynamics and information flow in a data-driven model of the primary motor cortex microcircuit. bioRxiv. 2019. p. 201707. doi:10.1101/201707

37. Neymotin SA, Suter BA, Dura-Bernal S, Shepherd GMG, Migliore M, Lytton WW. Optimizing computer models of corticospinal neurons to replicate in vitro dynamics. J Neurophysiol. 2017;117: 148–162.

38. Neymotin SA, Daniels DS, Caldwell B, McDougal RA, Carnevale NT, Jas M, et al. Human Neocortical Neurosolver (HNN), a new software tool for interpreting the cellular and network origin of human MEG/EEG data. Elife. 2020;9: 740597.

39. Neymotin SA, Lazarewicz MT, Sherif M. Ketamine disrupts theta modulation of gamma in a computer model of hippocampus. Journal of. 2011. Available: http://www.jneurosci.org/content/31/32/11733.short

40. Whittington MA, Traub RD, Kopell N, Ermentrout B, Buhl EH. Inhibition-based rhythms: experimental and mathematical observations on network dynamics. Int J Psychophysiol. 2000;38: 315–336.

41. Skinner FK, Kopell N, Marder E. Mechanisms for oscillation and frequency control in reciprocally inhibitory model neural networks. J Comput Neurosci. 1994;1: 69–87.

42. Vierling-Claassen D, Cardin JA, Moore CI, Jones SR. Computational modeling of distinct neocortical oscillations driven by cell-type selective optogenetic drive: separable resonant circuits controlled by low-threshold spiking and fast-spiking interneurons. Front Hum Neurosci. 2010;4: 198.

43. Fukunaga I, Herb JT, Kollo M, Boyden ES, Schaefer AT. Independent control of gamma and theta activity by distinct interneuron networks in the olfactory bulb. Nat Neurosci. 2014;17: 1208–1216.

44. Chen G, Zhang Y, Li X, Zhao X, Ye Q, Lin Y, et al. Distinct Inhibitory Circuits Orchestrate Cortical beta and gamma Band Oscillations. Neuron. 2017;96: 1403–1418.e6.

45. Cardin JA. Dissecting local circuits in vivo: integrated optogenetic and electrophysiology approaches for exploring inhibitory regulation of cortical activity. J Physiol Paris. 2012;106: 104–111.

46. Cardin JA, Carlén M, Meletis K, Knoblich U, Zhang F, Deisseroth K, et al. Driving fast-spiking cells induces gamma rhythm and controls sensory responses. Nature. 2009;459: 663–667.

47. Naka A, Veit J, Shababo B, Chance RK, Risso D, Stafford D, et al. Complementary networks of cortical somatostatin interneurons enforce layer specific control. Elife. 2019;8. doi:10.7554/eLife.43696

48. Feingold J, Gibson DJ, DePasquale B, Graybiel AM. Bursts of beta oscillation differentiate postperformance activity in the striatum and motor cortex of monkeys performing movement tasks. Proc Natl Acad Sci U S A. 2015;112: 13687–13692.

49. Little S, Bonaiuto J, Barnes G, Bestmann S. Human motor cortical beta bursts relate to movement planning and response errors. PLoS Biol. 2019;17: e3000479.

50. Wessel JR. β-Bursts Reveal the Trial-to-Trial Dynamics of Movement Initiation and Cancellation. J Neurosci. 2020;40: 411–423.

51. Lundqvist M, Herman P, Warden MR, Brincat SL, Miller EK. Gamma and beta bursts during working memory readout suggest roles in its volitional control. Nat Commun. 2018;9: 394.

52. Lakatos P, Shah AS, Knuth KH, Ulbert I, Karmos G, Schroeder CE. An oscillatory hierarchy controlling neuronal excitability and stimulus processing in the auditory cortex. J Neurophysiol. 2005;94: 1904–1911.

53. Sirota A, Montgomery S, Fujisawa S, Isomura Y, Zugaro M, Buzsáki G. Entrainment of neocortical neurons and gamma oscillations by the hippocampal theta rhythm. Neuron. 2008;60: 683–697.

54. Dvorak D, Fenton AA. Toward a proper estimation of phase–amplitude coupling in neural oscillations. J Neurosci Methods. 2014. Available: https://www.sciencedirect.com/science/article/pii/S0165027014000132

55. O'Connell MN, Barczak A, Ross D, McGinnis T, Schroeder CE, Lakatos P. Multi-Scale Entrainment of Coupled Neuronal Oscillations in Primary Auditory Cortex. Front Hum Neurosci. 2015;9: 655.

56. Tort ABL, Kramer MA, Thorn C, Gibson DJ, Kubota Y, Graybiel AM, et al. Dynamic cross-frequency couplings of local field potential oscillations in rat striatum and hippocampus during performance of a T-maze task. Proc Natl Acad Sci U S A. 2008;105: 20517–20522.

57. Bahramisharif A, van Gerven MAJ, Aarnoutse EJ, Mercier MR, Schwartz TH, Foxe JJ, et al.

Propagating neocortical gamma bursts are coordinated by traveling alpha waves. J Neurosci. 2013;33: 18849–18854.

58. Thut G, Miniussi C, Gross J. The functional importance of rhythmic activity in the brain. Curr Biol. 2012;22: R658–63.

59. Kayser C, Montemurro MA, Logothetis NK, Panzeri S. Spike-phase coding boosts and stabilizes information carried by spatial and temporal spike patterns. Neuron. 2009;61: 597–608.

60. Harris KD, Henze DA, Hirase H, Leinekugel X, Dragoi G, Czurkó A, et al. Spike train dynamics predicts theta-related phase precession in hippocampal pyramidal cells. Nature. 2002;417: 738–741.

61. Strauß A, Wöstmann M, Obleser J. Cortical alpha oscillations as a tool for auditory selective inhibition. Front Hum Neurosci. 2014;8: 350.

62. Klimesch W, Sauseng P, Hanslmayr S. EEG alpha oscillations: The inhibition–timing hypothesis. Brain Res Rev. 2007;53: 63–88.

63. Canavier CC. Phase-resetting as a tool of information transmission. Curr Opin Neurobiol. 2015;31: 206–213.

64. Doelling KB, Arnal LH, Ghitza O, Poeppel D. Acoustic landmarks drive delta-theta oscillations to enable speech comprehension by facilitating perceptual parsing. Neuroimage. 2014;85 Pt 2: 761–768.

65. Molinaro N, Lizarazu M. Delta(but not theta)-band cortical entrainment involves speech-specific processing. Eur J Neurosci. 2018;48: 2642–2650.

66. Peelle JE, Davis MH. Neural Oscillations Carry Speech Rhythm through to Comprehension. Front Psychol. 2012;3: 320.

67. Groppe DM, Bickel S, Dykstra AR, Wang X, Mégevand P, Mercier MR, et al. iELVis: An open source MATLAB toolbox for localizing and visualizing human intracranial electrode data. J Neurosci Methods. 2017;281: 40–48.